

Large Eddy Simulations of the Darmstadt Turbulent Stratified Flames with REDIM Reduced Kinetics

Ping Wang¹ · Tian-zeng Hou² · Cai-jun Wang² ·
Gerd Steinhilber³ · Ulrich Maas³

Received: 29 August 2017 / Accepted: 5 March 2018 / Published online: 18 May 2018
© Springer Science+Business Media B.V., part of Springer Nature 2018

Abstract Turbulent stratified combustion is often found in practical combustion devices, however, for large eddy simulations (LES) of it is still a challenge. In the present work, LES of the Darmstadt turbulent stratified flame (TSF) cases are conducted. In total, one isothermal flow case A-i2 and four reacting cases with different combinations of stratification and shear, i.e., A-r, C-r, E-r, G-r cases, are simulated. The employed sub-grid scale (SGS) combustion model is the REDIM-PFDF model, in which the chemical kinetics is reduced into a two-dimensional chemistry look-up table by the reaction-diffusion manifolds (REDIM) method, which performs a model reduction based on the coupling of the chemical kinetics with molecular transport. The fluctuation of scalars within the LES filter volume is modeled by the presumed filtered density function (PFDF). The overall good agreement of the statistics of velocity, temperature and species with the experimental data demonstrates the capability of the REDIM-PFDF model for TSF. Additionally, the probability distributions of the alignment angle, α , between the reaction layer and mixing layer, are analyzed in detail. It is shown that the probability distributions of the alignment angle vary with the axial distance from the jet nozzle. It also reveals that, with a stronger turbulence, the stratification effect can be weakened and the probability difference for finding ‘back-supported’ and ‘front-supported’ flame modes tends to decrease.

Electronic supplementary material The online version of this article (<https://doi.org/10.1007/s10494-018-9899-1>) contains supplementary material, which is available to authorized users.

✉ Ping Wang
pingwang@ujs.edu.cn

¹ Institute for Energy Research, Jiangsu University, Xuefu Road 301, Zhenjiang, 212013 China

² School of Energy and Power Engineering, Jiangsu University, Xuefu Road 301, Zhenjiang, 212013, China

³ Institut für Technische Thermodynamik, Karlsruher Institut für Technologie, Kaiserstr. 12, D-76131 Karlsruhe, Germany

Keywords REDIM · Tabulated chemistry · Stratified flame · Turbulent combustion · Large eddy simulations · Alignment angle

1 Introduction

Lean premixed combustion is often used to reduce emission. However, it is prone to combustion instability [1]. One approach to cope with this is to create an intentionally spatially non-uniform reactant mixture distribution [2]. Although the global equivalence ratio is small, locally combustion of rich reactant mixtures can be used as a heat source to ignite adjacent leaner mixtures, hence stabilizing the flame. In this situation, local equivalence ratio varies significantly, which is very different to idealized premixed and diffusion flames.

Large eddy simulations (LES) are a promising tool for dealing with turbulent combustion [3–10]. However, LES of stratified combustion and partially premixed combustion still constitutes an open challenge [2, 11]. One of the keys to LES of turbulent combustion is how to account for detailed chemistry, since the use of detailed chemistry directly in LES is prohibitive [12–14], or at least computationally very demanding. To overcome this difficulty, various mechanism reduction schemes exist [15–17]. A recently developed scheme is the reaction-diffusion manifolds (REDIM) method [18, 19], which is based on its predecessor, Intrinsic Low-Dimensional Manifolds (ILDM), where the chemical dynamics is decomposed into processes corresponding to various time scales [20]. In contrast to ILDM, REDIM explicitly takes into account the coupling of chemical reaction and molecular transport processes. With REDIM, a thermo-chemical state is described in a simplified way by a few (typically, one to three) reduced variables, on which the remaining variables (including the chemical source terms) depend. The Flame Prolongation of ILDM (FPI) [21] and Flamelet Generated Manifold (FGM) [22, 23] techniques are two related alternative approaches to downsize combustion chemistry by using trajectories in composition space obtained from the calculations of laminar flames.

LES do not fully resolve the velocity and scalar field; nevertheless, they allow to analyze the interaction of flow, mixing and chemical reaction. For the stratified combustion, the alignment angle α ($0-\pi$) between mixing layer and reaction layer, as defined in Fig. 1 in [24] under ideal condition or in a real turbulent flow field as shown in Fig. 1, is an important quantity, which can indicate the ‘back- or front-supported’ flame propagating modes depending on the value of it. When the flame propagates toward leaner mixture ($\alpha < \pi/2$), it represents ‘back-supported’ flame and vice versa. In early studies, Dar Cruz et al. [25] conducted a series of simulations of one-dimensional laminar flames under spatially stratified equivalence ratio conditions by employing detailed chemistry, and it is observed that an enhanced flame propagation and extended flammability limit can be obtained in the ‘back-supported’ flame. Jiménez et al. [26] performed a two-dimensional detailed chemistry Direct Numerical Simulation (DNS) for global lean stratified propane-air flames, in which a weakened effect of stratification due to mixing process was addressed briefly. Later, several turbulent annular stratified flames stabilized by weak swirl were measured with the advanced laser diagnostics methods by Bonaldo and Kelman [27]. These measurements demonstrated that an increased turbulence can result in a faster mixing between the flow components and consequently a decreased effect of stratification.

Most recently, several novel designed stratified burners [24, 28, 29] have been investigated with the aid of advanced measurement techniques, aiming to provide abundant experimental data for model validation. For the benchmark Darmstadt turbulent stratified flame (TSF), Seffrin et al. [30] have studied numerous test configurations, since the flow

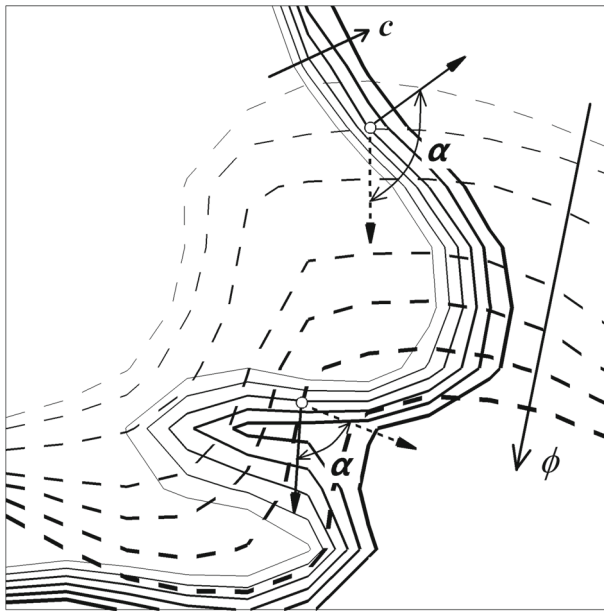


Fig. 1 Diagrammatic sketch of the alignment angle α between the gradient vectors of the equivalence ratio ϕ and the progress variable c , generated from the present obtained LES results. Arrows indicate the increase of the values according to the contour levels

rate and the equivalence ratios can be adjusted independently. They find different flame structures and provide abundant experimental data for others to simulate the TSF. A series of detailed measurements of the four cases of the TSF have been done by Böhm et al. [31]. Kuenne et al. [24], and they also analyzed the TSF both experimentally and numerically by using 1D Raman/Rayleigh scattering and LES with tabulated chemistry combined with a thickened flame approach. Up to now several LES of the Darmstadt TSF have been performed [24, 32–36] with different sub-grid scale (SGS) combustion models. The used models include a fractal flame wrinkling flame surface density model [34], a coupled level set/progress variable model [32, 35], the F-TACLES model [36] and an artificially thickened flame model coupled with FGM [24, 33]. Recently, Fiorina et al. [11] performed a detailed performance assessing study of five SGS combustion models via LES of the Darmstadt TSF A-r case. These five models are implemented in different codes and by different research groups, and it is demonstrated that the five models perform different in many aspects. In the previous simulations of Darmstadt TSF, however, the impact of turbulence strength on the stratified flame propagating mode and stratification has not yet been investigated in depth.

In this work, four Darmstadt TSF reacting cases, with different combination of stratification and shear, i.e., A-r, C-r, E-r, G-r cases, will be investigated numerically by a SGS combustion model, which is different from those used in the previous work [11, 24, 32–36]. The used model is a combination of the 2d-REDIM chemistry table and the presumed filtered probability density function (PFDF) method, which has been applied on the simulation of turbulent premixed combustion inside the PRECCINSTA burner [37] and on the simulation of partially premixed flames near extinction [38].

The outline of the paper is as follows. A brief description of the generation of the used 2d-REDIM chemistry table will be given in Section 2, and followed by a summary of the

used combustion model and numerical method in Section 3. Next, the burner geometry and computational set-up is explained to provide information on the geometry and the boundary conditions employed. Finally, a detailed analysis of the obtained flow field and statistic results is presented in Section 5.

2 REDIM Chemistry Table

The chemical kinetics for simulating Darmstadt TSF is simplified with the REDIM method [18, 19]. According to recently reported investigations [19], a two-dimensional manifold can be used as a reduced system with good accuracy, such that the kinetics in the LES can be described with the mass fractions of N_2 (representing mixing state) and CO_2 (representing reaction progress). For the identification of the manifold, a detailed mechanism for methane combustion with 34 species [39] was used with equal diffusivities of the species and unity Lewis number assumption, which is an acceptable simplification for methane combustion. The effects of preferential diffusion are weak in the case of methane combustion, particularly under lean conditions [40]. Note that REDIM can also be constructed without using this assumption [41].

The REDIM is obtained via the solution of an evolution equation for a low-dimensional manifold in the thermo-kinetic space [19]:

$$\frac{\partial \psi}{\partial t} = (I - \psi_{\theta} \psi_{\theta}^+) \{ F(\psi) + \frac{d}{\rho} \chi \circ \psi_{\theta\theta} \circ \chi \} \quad (1)$$

The thermo-kinetic space is described by a vector Ψ , which is a function of one or multiple reduced coordinates, given by the vector θ . The variable ρ is density, χ is the vector of spatial gradient estimates for θ , $F(\Psi)$ is the vector of the chemical source terms, Ψ_{θ} is the matrix of partial derivatives of Ψ with respect to θ and ψ_{θ}^+ is its Moore-Penrose pseudo-inverse, $\Psi_{\theta\theta}$ is the Hessian matrix. The symbol ‘ \circ ’ in Eq. 1 is an abbreviation for the multiplication of two vectors with a tensor of third order. The process for obtaining an REDIM chemistry table consists of four sub-steps:

- 1) specify the spatial gradient χ as a function of θ ;
- 2) specify the initial and boundary conditions for Eq. 1;
- 3) integrate Eq. 1 in time until a steady state $\Psi(\theta)$ is obtained;
- 4) store the manifold data, i.e. Ψ_{θ} , $\Psi(\theta)$, ψ_{θ}^+ , $F(\Psi(\theta))$, such that it can be used in a subsequent simulation.

More detailed information about the REDIM chemistry table generation can be found in [19].

As shown in above, in order to solve the Eq. 1, the spatial gradients, χ , should be given firstly. It can be determined by an iteration method [19]. For the present work, it was motivated from physical considerations for stratified flames. In a simplified picture the stratified combustion may be regarded as premixed flames that interact through mixing within the flow field. Therefore, the estimation of gradients was based on a gradient of CO_2 from premixed flames and a constant value for the gradient of N_2 to respect the mixing within the flow field. The latter was taken as an average value for the extinction of a premixed flame due to mixing with air. Although this is a very simple estimation for the gradients, in principle it already respects the situation in stratified flames to lie between the extreme cases of premixed and non-premixed combustion, as analyzed in [19]. Therefore, the REDIM method appears as a suitable choice for this combustion regime, where typical flamelet

methods may have limitations [42]; however, extensions of the flamelet concept can solve these problems [23, 43].

For the Darmstadt TSF under consideration [30, 31], two reduced coordinates are used in this work, namely, the mass fraction of CO₂ and N₂. All other species, density, temperature as well as production rate of CO₂ and so on, can be determined from the lookup table. Figure 2 shows the tabulated production rate of CO₂ and mass fraction of CO, as a function of CO₂ and N₂ mass fraction, given by the used REDIM chemistry table. In Fig. 2, zero CO₂ mass fraction means non-reacting reactant mixture, while minimum N₂ value (0.726) represents the equivalence ratio $\varphi=0.9$ state. The CO₂ and N₂ can physically only vary in a limited triangle zone (the region over the solid straight line in Fig. 2), but for convenience of numerical simulation the REDIM table is extended to be a rectangular region.

It is interesting to note here, the REDM method bears similarities to the CMC [44] and MMC [45] method in that it conditions the minor species on the mixture fraction and the progress variable (based on the magnitude of the gradient). In this way, the coupling of diffusion with chemical reaction is incorporated into the model in a natural way.

3 Combustion Model and Numerical Method

In LES calculation, the transport equations are solved for continuity, momentum and mass fractions of CO₂ and N₂. The Favre filtered transport equation for the mass fraction is:

$$\frac{\partial \bar{\rho} \tilde{Y}_k}{\partial t} + \frac{\partial}{\partial x_i} (\bar{\rho} \tilde{u}_i \tilde{Y}_k) + \frac{\partial}{\partial x_i} (\overline{\rho u_i Y_k} - \bar{\rho} \tilde{u}_i \tilde{Y}_k) = \frac{\partial}{\partial x_i} (\bar{\rho} \bar{D} \frac{\partial \tilde{Y}_k}{\partial x_i}) + \bar{\rho} \tilde{\omega}_k \quad (2)$$

where the index $k = 1, 2$ denotes CO₂ and N₂, respectively. Note that for N₂ the source term in Eq. 2 is zero. The Favre filtered production rate is determined from the pre-calculated REDIM/FDF table employing the presumed joint filtered density function (FDF) method. Compared to the presumed FDF method, the exact FDF can be calculated by solving additional FDF transport equations [46, 47] in the transported FDF method, which is more general and copes better with the fact that the variables are normally not statistically independent. The transported FDF method, however, is still considered too expensive for routine LES calculations. With the presumed FDF method, the general shape of the FDF is devised

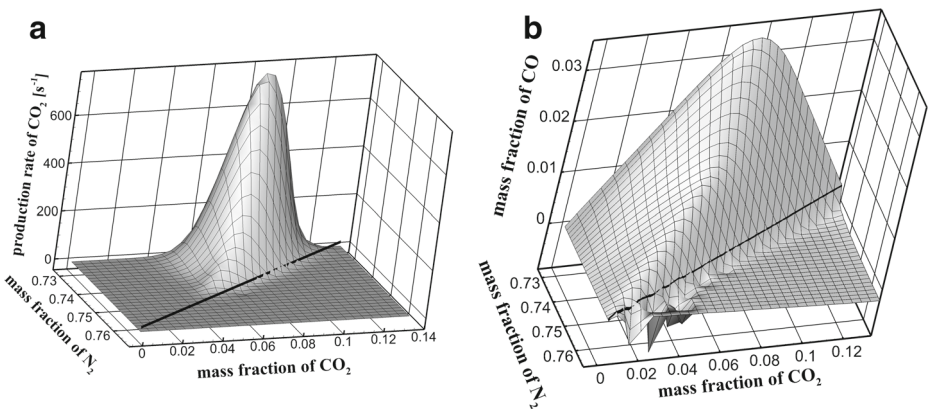


Fig. 2 The used REDIM chemistry table for **a** production rate of CO₂, and **b** mass fraction of CO, as a function of mass fractions of CO₂ and N₂

a priori, and it is parameterized in terms of low moments, usually the mean and the variance. This method is cheaper, and still it has been shown to provide satisfactory results [48, 49].

The generation of the pre-calculated REDIM/FDF table is described below. The assumption of statistical independence of Y_1 and Y_2 is employed in this work, which leads to the joint FDF being equal to the product of the two marginal FDFs, i.e. $\tilde{P}(Y_1, Y_2) = \tilde{P}(Y_1)\tilde{P}(Y_2)$. In this work, both $\tilde{P}(Y_1)$ and $\tilde{P}(Y_2)$ are presumed to be Clipped Gaussian FDF. This is different from the shapes adopted in [50], where a β PDF was used for the mixture fraction while for the progress variable a double- delta PDF was used. It is believed that the double-delta PDF is suitable for $\tilde{P}(Y_{CO_2})$ in the rapid combustion where an infinitely thin flame can be assumed. The β PDF on the other hand is known to be good for a mixture fraction type of scalar [51], but it is rarely used for reaction progress variable such as the reactive scalar Y_{CO_2} here [52]. In the previous work [37], two presumed FDFs: Top-hat and Clipped Gaussian, have been used separately with the 1d-REDIM table to calculate the well-known PRECCINSTA premixed flames [53], and it was found that the LES results are not very sensitivity to the shapes of the presumed FDFs, as reported in [48–54].

For the presumed Clipped Gaussian FDF, $\tilde{P}(Y_1)$ and $\tilde{P}(Y_2)$ are determined by the mean and the variance, i.e., $(\tilde{Y}_{CO_2}, \tilde{Y}_{CO_2}''')$ and $(\tilde{Y}_{N_2}, \tilde{Y}_{N_2}''')$, respectively. The mean value is obtained from Eq. 2 while the variance is modeled algebraically [48]. The mean and variance of Y_α are then used to determine the joint FDF, $\tilde{P}(Y_1, Y_2)$. For a general scalar variable f , depending on (Y_1, Y_2) , its Favre filtered quantity at given \tilde{Y}_α and \tilde{Y}_α''' is found with the aid of the joint FDF, as in [55, 56] via:

$$\tilde{f} = \int_{Y_{1,\min}}^{Y_{1,\max}} \int_{Y_{2,\min}}^{Y_{2,\max}} f(Y_1, Y_2) \tilde{P}(Y_1) \tilde{P}(Y_2) dY_1 dY_2 \quad (3)$$

while the Reynolds-filtered density is calculated via

$$\frac{1}{\tilde{\rho}} = \int_{Y_{1,\min}}^{Y_{1,\max}} \int_{Y_{2,\min}}^{Y_{2,\max}} \frac{1}{\rho(Y_1, Y_2)} \tilde{P}(Y_1) \tilde{P}(Y_2) dY_1 dY_2 \quad (4)$$

The results calculated via (3) and (4), are tabulated with points $31 \times 11 \times 26 \times 11$ for $\tilde{Y}_{CO_2} \times \tilde{Y}_{CO_2}''' \times \tilde{Y}_{N_2} \times \tilde{Y}_{N_2}'''$.

The pre-calculated REDIM/FDF look-up table was employed in the in-house Finite-Volume code LESOCC2C [57]. It is highly vectorized and parallelized by domain decomposition and explicit message passing via MPI. The code solves the Low-Mach-number version of the compressible Navier-Stokes equations on body-fitted curvilinear block-structured grids using second-order central schemes in space and a three-step Runge-Kutta method of second order in time. The convection term of the species equation was discretized with the HPLA scheme [58]. The variable-density dynamic Smagorinsky model is used to determine the SGS eddy viscosity in the Favre filtered momentum equation. The SGS scalar flux is modeled by a gradient diffusion model, with turbulent Schmidt number 0.7 [57].

4 Burner Configuration and Numerical Setup

The above numerical method is used to simulate the Darmstadt stratified burner [30, 31]. The burner consists of three concentric tubes surrounded by an air coflow, as shown in Fig. 3. The inner diameters of the 3 tubes are 14.8 mm, 37 mm and 60 mm, respectively, and the tube length is 500 mm. The central tube acts as the pilot, and a flame holder ring is constructed inside it. Seffrin et al. [30] have studied numerous test configurations, since

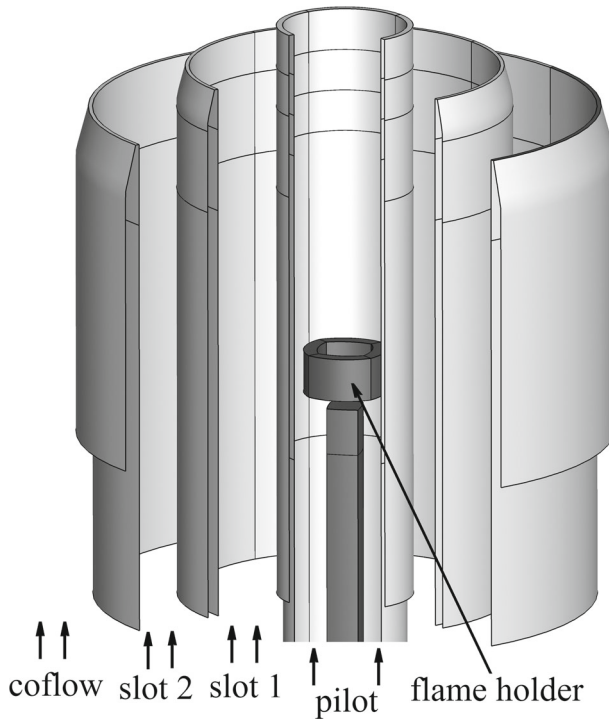


Fig. 3 Sketch of the stratified flame burner

the flow rates and equivalence ratios can be adjusted independently of the pilot and of each slot. In the present work, an isothermal flow case (A-i2) and four reacting cases (A-r, C-r, E-r, G-r) are simulated. The main information for these cases is summarized in Table 1.

The 3-dimensional computational domain is similar to the burner set-up described in [30, 31], and it includes the flame holder inside. The mesh used is a body-fitted multi-block structured grid that includes the 3 tubes jet inflow channel and a round domain enclosing the flame. This round domain extends to 1600 mm downstream with a diameter of 600 mm. The whole domain is divided into 308 blocks, and the solid lines in Fig. 3 show the block boundaries at the burner surface (except the flame holder). The mesh is first generated with

Table 1 Flow parameters for the 5 cases simulated in the present work

Case	φ_{pilot}	u_{pilot}	Re_{pilot}	φ_{slot1}	u_{slot1}	Re_{slot1}	φ_{slot2}	u_{slot2}	Re_{slot2}	u_{coflow}
A-i2	0	10	9800	0	10	13,800	0	10	13,300	0.1
A-r	0.9	1	980	0.9	10	13,800	0.6	10	13,300	0.1
C-r	0.9	1	980	0.9	10	13,800	0.6	5	6,700	0.1
E-r	0.9	1	980	0.9	10	13,800	0.9	5	6,700	0.1
G-r	0.9	1	980	0.9	10	13,800	0.9	10	13,300	0.1

Bulk velocities u (m/s), equivalence ratios φ (–), Reynolds numbers Re (–) (based on the bulk velocity and hydraulic diameter) All bulk velocities are calculated using the unburnt gas density and the corresponding tube exit area, as described in [24]

O-type grid method using ICEM-CFD software, by neglecting the flame holder in the pilot pipe. The solid body of flame holder is then dug out from the mesh by a special mesh post processing technology. A grid resolution study is performed using two grids with 1.2 and 2.6 million cells, respectively. The fine grid corresponding to a local refinement of the coarse grid in the region near the jet exits, $x < 336$ mm and $r < 30$ mm, mainly in streamwise and radial directions, is shown in Fig. 4 as well as the coarse grid. In the fine grid, at the vicinity of the pilot nozzle the grid size is around 0.5, 0.6, 0.5 mm in axial, tangential and radial directions, respectively.

A convective outflow boundary condition is imposed at the exit, and a uniform velocity profile without fluctuations is used at the inlet of the coflow. A separate simulation of turbulent pipe flow with streamwise periodic condition is performed simultaneously as described in [57] to obtain the fully developed turbulent flow as described in [30], in the 3 tubes upstream of the jet exit. The periodic calculation inflow pipes are ranged in $x \in [-127, -52]$, $x \in [-70, -20]$ and $x \in [-70, -20]$ mm in axial direction for the pilot, slot 1 and slot 2, respectively, as shadow shown in Fig. 5. The method of generating inflow turbulence is different from those in [24, 32–36], in which pseudo-turbulent inflow [34] or synthetically generated turbulence [33] was superimposed. For the walls, no-slip adiabatic boundary conditions are used, while for the lateral confinement, slip boundary conditions are used. The Werner-Wengle wall function [59] is used at the pipe walls. Note that in simulations of the reacting cases, fully burnt exhaust gas is charged in the pilot pipe, as done in [36], to avoid too fine grid cells near the flame holder. Accordingly, the bulk velocity of pilot pipe is adjusted to match the mass flow rate of the experiment.

5 Results and Discussion

5.1 Flow and flame structures

Snapshots of flow field of the isothermal and reacting cases at the vicinity of jet exit are shown in Fig. 6, obtained on the fine grid. It is seen from the corresponding time series

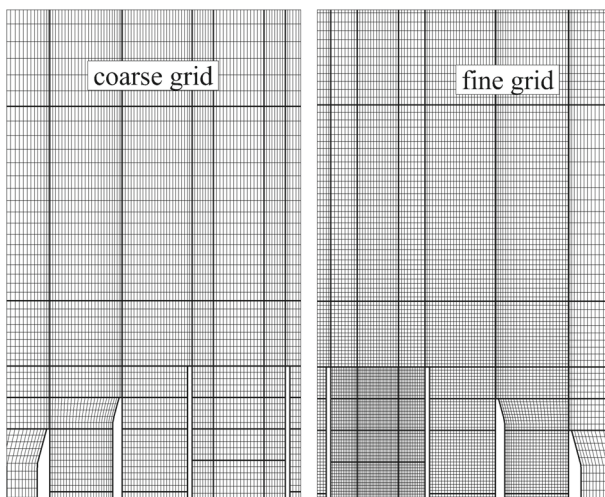


Fig. 4 The grid cell distributions in the vicinity of jet exits in center plane

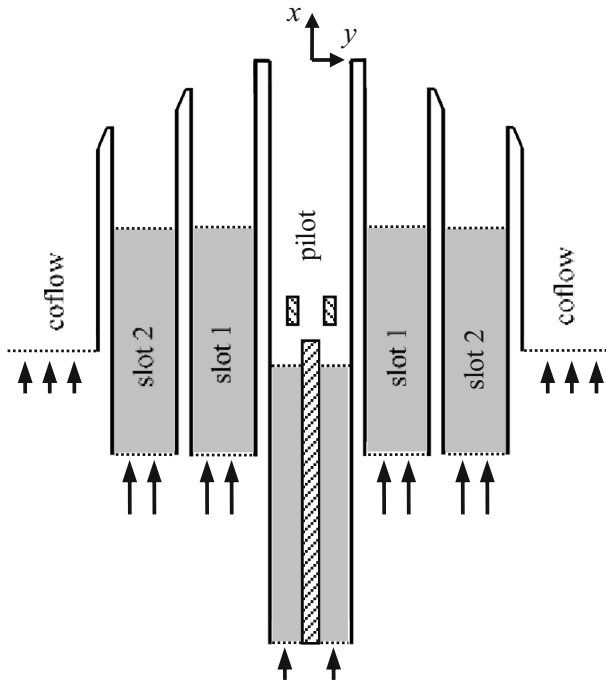


Fig. 5 Sketch of the computational domain, in which the shadow regions show the periodic calculation inflow pipes

of simulation results, as the snapshot shown in Fig. 6a, the turbulence is well developed by using periodic inlet flow condition in the three jet pipes of isothermal case, which is consistent with the experimental data and previous LES simulations [24]. However, the turbulence in the center pilot pipe has almost vanished for the reacting case because its bulk velocity is only one tenth of the isothermal case; hence, the Reynolds number is decreased greatly. This phenomenon is well presented in Fig. 6b. It is worth pointing out that the transition of laminar flow from pilot pipe to turbulence can be predicted well because of the used dynamic Smagorinsky SGS model. Due to heat expansion, the reacting case shows a wider jet spreading angle than the isothermal case.

Figure 7 shows 2D instantaneous snapshots of the resolved flame fronts for the four reactive cases. Here, the flame front is displayed by the iso-contour of production rate of CO_2 . Isolines of equivalence ratio are also displayed in Fig. 7, with value of 0.2, 0.4, 0.6 and 0.8, respectively. From Fig. 7 and the corresponding animations (included in the appendix materials), it is seen that the flame spreading angles and movements of the flame fronts for the four cases are very similar, in upstream region $x < 30$ mm. This confirms the findings in [31, 32]. Further downstream, the flames burning toward the fresh reactant mixture coming from slot 2. Due to the different combinations of the bulk velocity and equivalence ratio for the mixture ejected from slot 2, behaviors of the flame front are fairly different from each other. In case A-r, the equivalence ratio in slot 2 is 0.6 so that its burning velocity is lower than those of E-r and G-r cases, in which equivalence ratio is 0.9 in slot 2. Meanwhile, the bulk velocity of slot 2 in case A-r is larger than those in C-r and E-r cases. Considering the balance between the inflow speed of fresh reactant mixture and the flame propagating

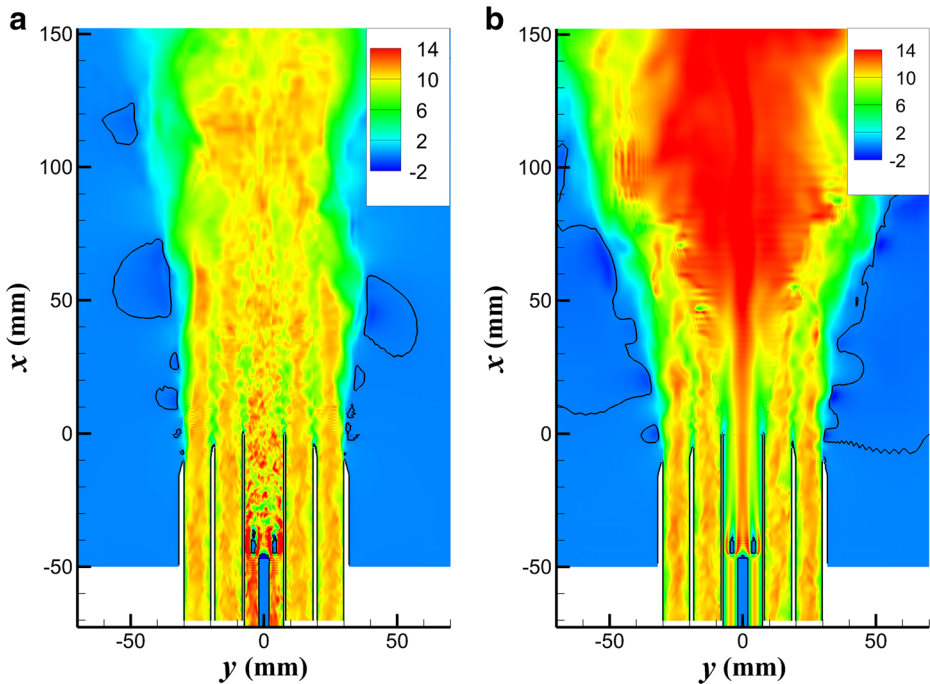


Fig. 6 Snapshots of streamwise velocity in the center plane obtained with LES on the fine grid. **a** case A-i2. **b** case A-r

speed normal to the flame front, it is expected that the flame front of case A-r has a smaller spreading angle compared with the other 3 cases. It is found from Fig. 7 that the shape of flame A-r is the slimmest and extended farthest downstream, which can be observed qualitatively in Fig. 2 of [30]. Based on the same consideration, it is also expected that E-r should have the shortest flame height among the 4 cases. In addition, Fig. 7 and the corresponding animations also show that the flame fronts, after $x = 50$ mm, are immense wrinkled, and even folded many times (C-r, E-r, G-r), which demonstrates a very complicated interaction between the stratified flame and turbulence.

Figure 8 shows the time averaged reaction layer and mixing layer for the four reacting cases. It can be observed that there is a stronger shear layer between slot 1 and slot 2 in case C-r (Fig. 8b) as compared with the case A-r (Fig. 8a), and this results a faster mixing of gasses from slot 1 and slot 2 and hence a weaker stratification effect. This is demonstrated by the wider spreading angle of the five isolines of equivalence ratio in Fig. 8b than in Fig. 8a. In other words, stronger turbulence can accelerate the mixing and therefore it impairs the stratification. It is also noticed that the flame brush of case A-r is thinner and extends further downstream than of case C-r. For the cases of E-r and G-r, since the difference of equivalence ratio is presented only between the slot 2 and the coflow air, the stratification effect on flame front is only shown in downstream region, i.e., $x > 50$ mm. The height of the flame brush of case G-r (Fig. 8d) is much larger than that of case E-r (Fig. 8c), which is thought to be as a result of the larger bulk velocity of slot 2 in case G-r.

A snapshot of the resolved three-dimensional flame front for the reacting cases A-r is shown in Fig. 9, represented by the isosurface of $T = 1500$ K, and colored by the local value

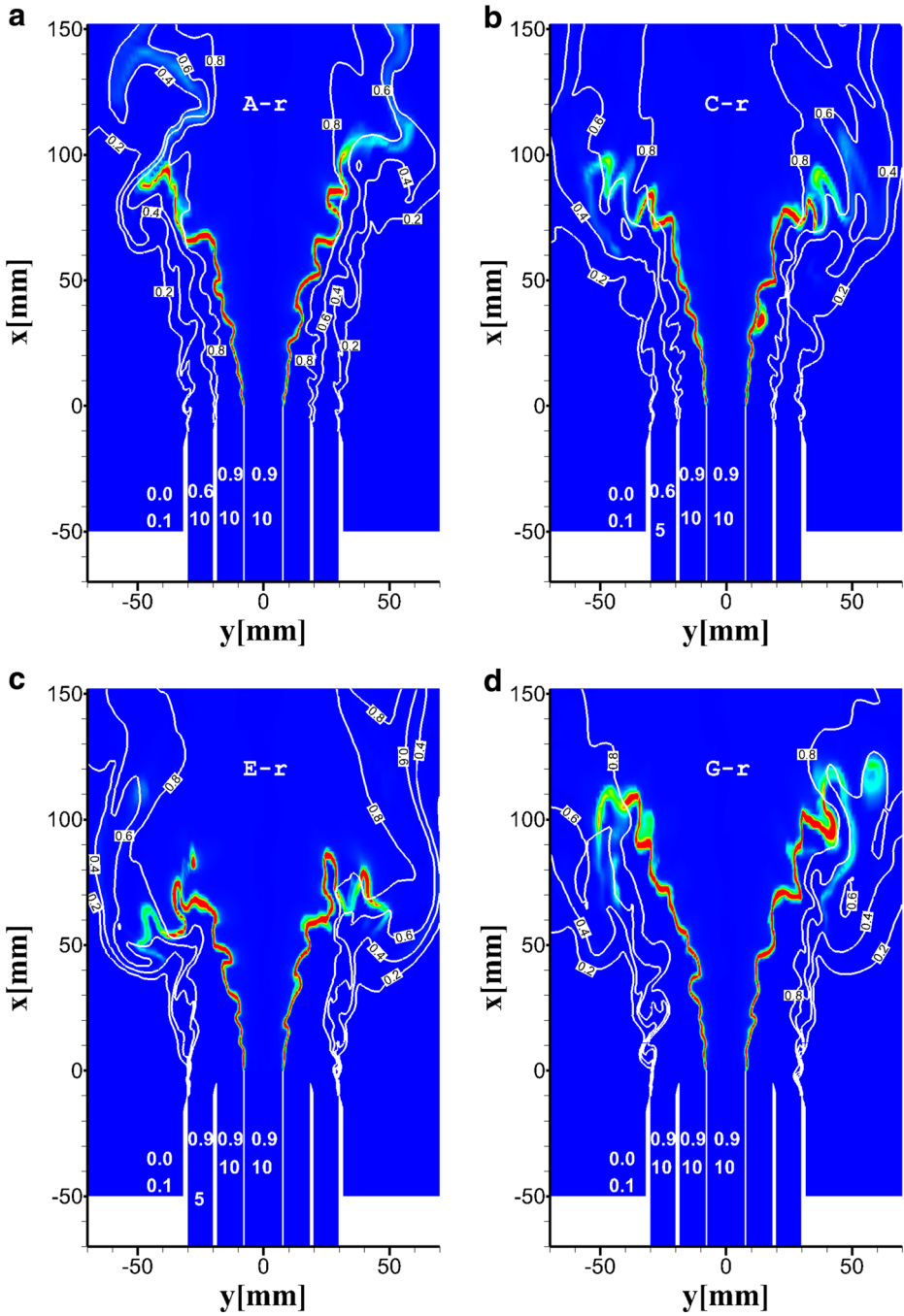


Fig. 7 Snapshots of the contour of CO₂ production rate, with solid curves showing isolines of equivalence ratio. The numbers in the 3 inflow pipes and coflow show the equivalence ratios (upper ones) and bulk flow speeds (lower ones), while numbers along isolines show the local equivalence ratio

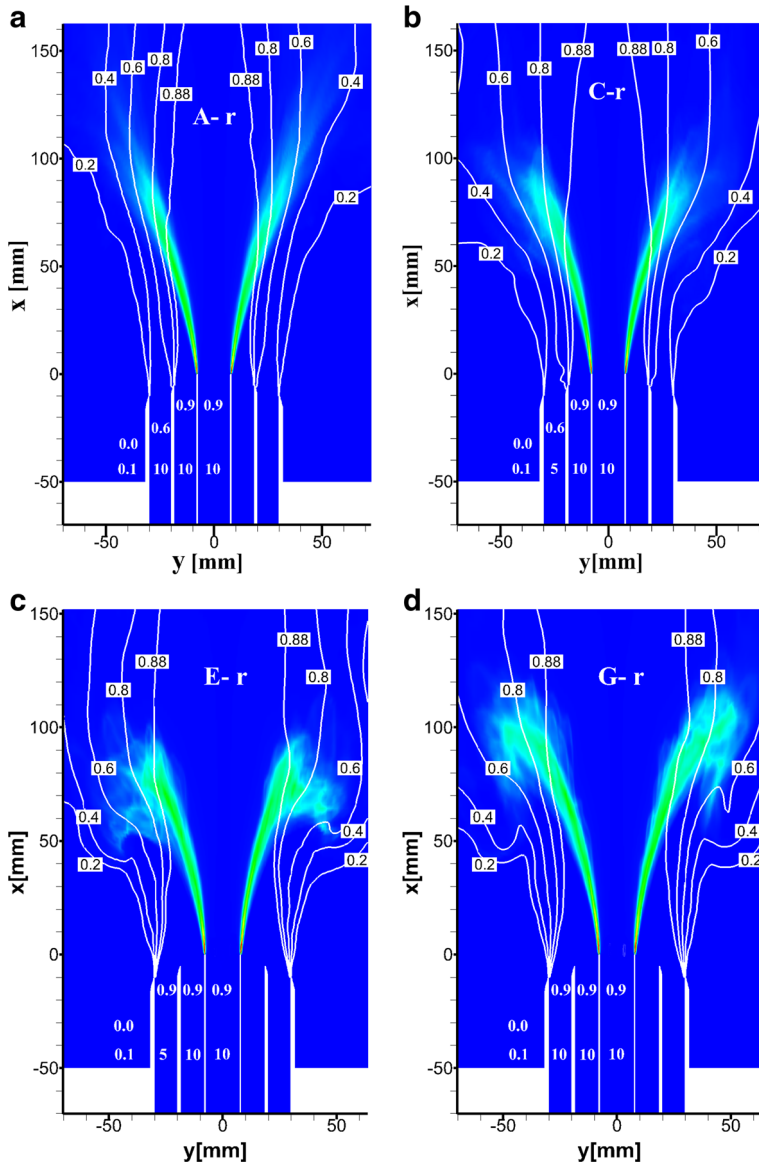


Fig. 8 Time averaged contours of CO_2 production rate. The solid curves show the isolines of equivalence ratio

of equivalence ratio. It is verified that the equivalence ratio on the flame front is always 0.9 in upstream region ($x < 40$ mm). However, it decreases steadily as the axial distance from the exit increase because the flame front starts to cross the mixing layer between the inner slot gas ($\varphi = 0.9$) and the outer slot gas ($\varphi = 0.6$). It is seen that the flame front is highly wrinkled by the strong turbulent flow, and at the same time the mixing layer is also distorted greatly. From Figs. 8 and 9, one might conclude that the flame propagating mode at different

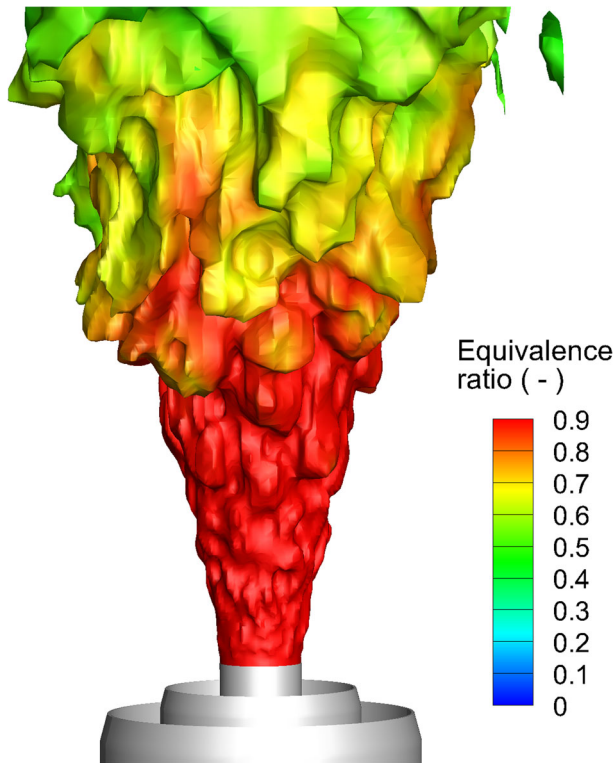


Fig. 9 Resolved instantaneous flame front ($T = 1500$ K) of case A-r, colored by the equivalence ratio

axial positions are completely different, since the crossing angle of reaction layer to the mixing layer is different and the equivalence ratio on the fame front is different too.

5.2 Statistics of velocity, temperature and species

Figure 10 shows the radial profiles of streamwise velocity for the isothermal case A-i2 at different axial positions. At axial position $x = 1$ mm, the three peaks of mean velocity in Fig. 10a demonstrate three jet flows. These peaks become less obvious with the development of the flow down to the stream. LES results obtained with the fine grid gives a slight better agreement with experimental data. Figure 11 shows profiles of streamwise velocity for the reacting case A-r. The discrepancy between the coarse and fine grid results is small, and the predicted mean streamwise velocities agree well with the experiment (Fig. 11a). However, Fig. 11b shows a large discrepancy in the rms profiles especially along the centerline. In the measurement [30], the velocity was measured by LDV and PIV techniques, and the pilot, both annular slots and the coflow were seeded with individual seeding generators. The measuremental error is possible relative larger along the centerline. In the previous study [11], five different SGS combustion models have been used to simulate the same A-r case, and it was found that the mean axial velocity profiles agree well with experiment data (see Fig. 6 of [11]), while for rms profiles the discrepancy between LES and experiment is also very large (see Fig. 8 of [11]).

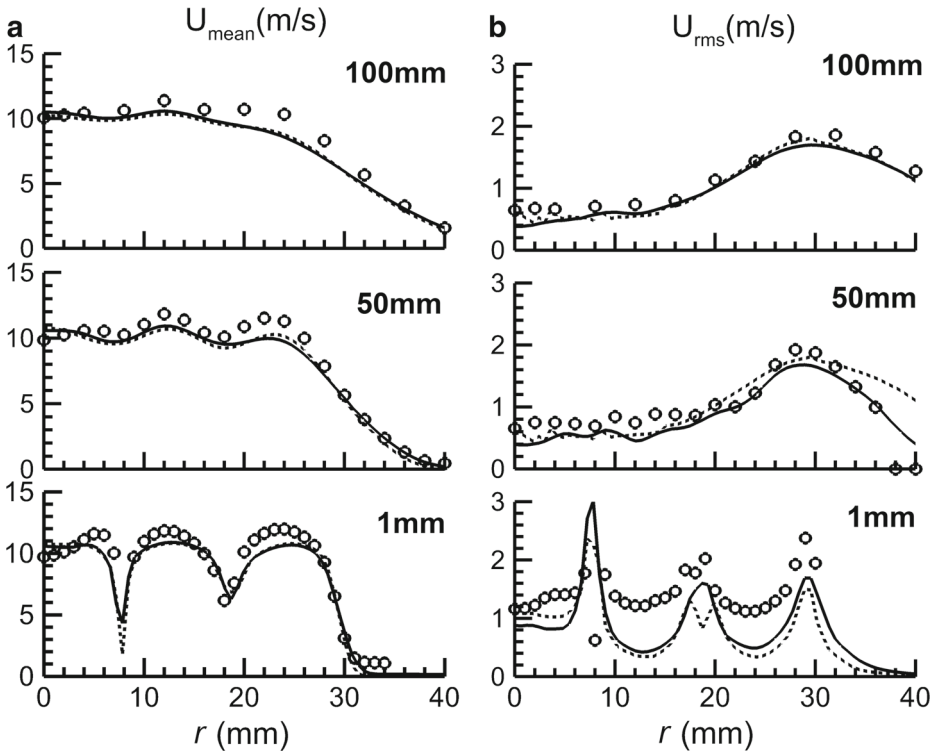


Fig. 10 Radial profiles of mean and rms fluctuation of streamwise velocity for case A-i2. ‘o’: experimental data; —: results on fine grid; - - results on coarse grid

Radial profiles of temperature and major species mass fraction statistics from the LES computations and the experimental data are shown in Figs. 12, 13, 14, 15 and 16. To provide a cross-comparison, the LES data extracted from Kuenne et al. [24] is displayed as well, in which LES was conducted with tabulated chemistry combined with a thickened flame approach.

For the radial profiles of temperature, the results are shown in Fig. 12. The overall tendency of mean temperature is predicted well, except at the lower axial position where the peak of temperature is overestimated significantly in the center. This is as a result of the heat loss to the pilot pipe in the measurement while adiabatic wall boundary condition is applied in LES. Trisjono et al. [35] simulated the same flame using a flamelet model with heat loss effect accounted for by an enthalpy defect approach. It was demonstrated that the incorporation of heat loss effect improves the agreement of temperature [35].

It is also seen in Fig. 12 that the LES results obtained with fine grid and coarse grid are very similar in many axial positions and agree well with experimental data. However, at $x = 75$ mm and 100 mm locations, the fine grid results are much better than the coarse grid results. This possible hints that the interaction between the flame and turbulence is particularly complex in the range of $75 \text{ mm} < x < 100 \text{ mm}$. In this region, the reaction is not as fast as in upstream (equivalence ratio is higher in upstream), and both the turbulent mixing process and the reaction play an important role on the flow behavior. This constitutes a tough challenge for the SGS combustion modeling, and a higher grid resolution is preferred

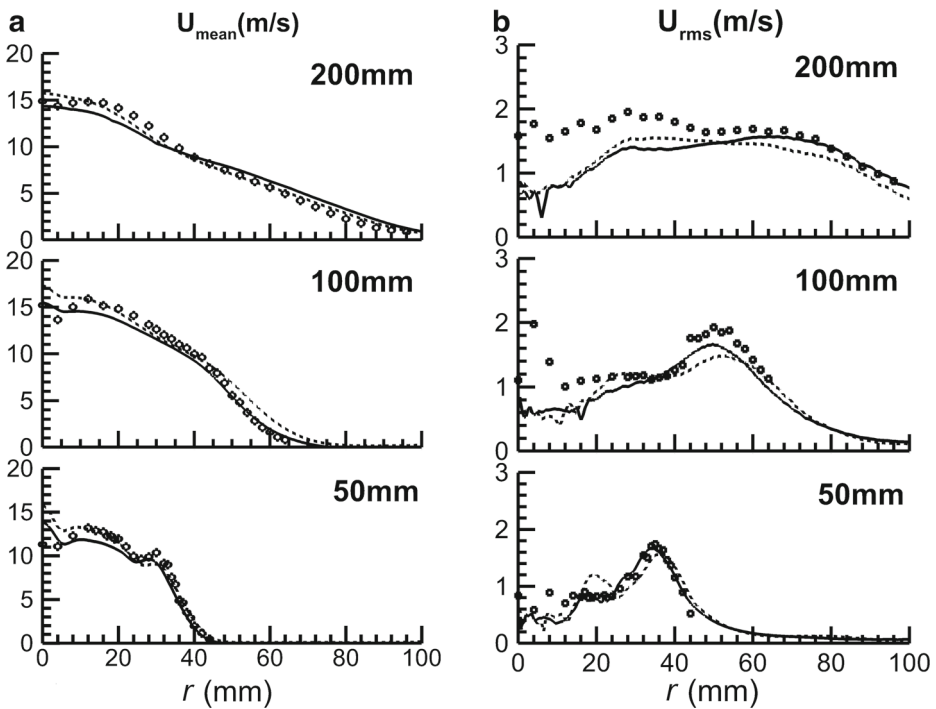


Fig. 11 Radial profiles of mean and rms fluctuation of streamwise velocity for case A-r. ‘o’: experimental data; —: results on fine grid; - - results on coarse grid

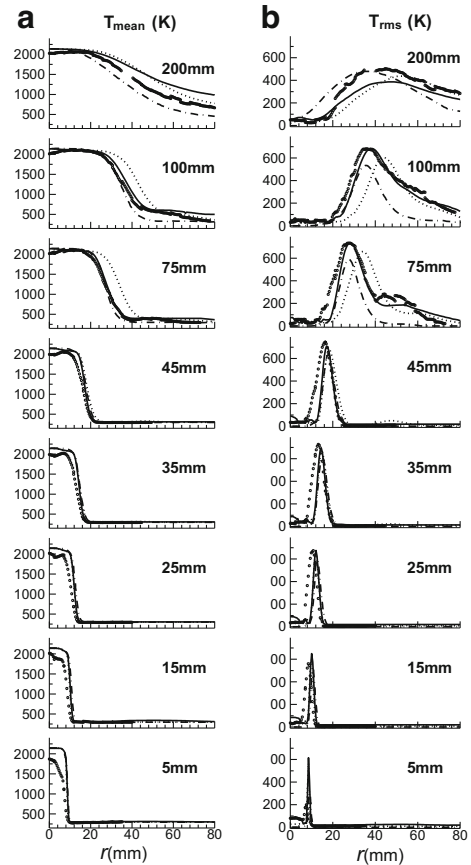
to relax this challenge. In the further downstream, $x > 150$ mm, no flame front is present, while only pure mixing of the hot exhaust with cold coflow air is taking place there.

Overall the width of the peak of temperature rms fluctuation (Fig. 12b) reveals the thickness of the flame brush. Near the pilot exit, the flame brush is very narrow due to the anchoring effect on the flame root [60]. Downstream, the thickness of the flame brush increases as well as the width of peak of T_{rms} .

Figures 13 and 14 show radial profiles of the main products of the combustion, CO_2 and H_2O , respectively. Unlike the over predicted temperature in the center at the lower axial positions, $x \leq 45$ mm, the predicted mean profiles of CO_2 (Fig. 13a) agree well with the experimental data. Both the experiment and LES results reach the equilibrium value along the centerline, which confirms that the chemical reaction is completed in the hot exhaust of pilot flame and the hot gas cools down afterwards due to heat loss to the environment, as explained in [24]. The same tendency is also found for the mean H_2O mass fraction (Fig. 14a). It is shown in Figs. 13b and 14b, the agreement between the predicted rms fluctuations of main reaction products and the experiment data is also satisfactory at the lower axial positions, $x \leq 45$ mm. The discrepancy between the LES results of fine grid and coarse grid is small in these locations. However, at further downstream $x \geq 75$ mm, the discrepancies between LES results of fine grid and coarse grid, and between the LES results and experiment are much larger than in upstream. This tendency is similar to that of temperature profiles.

Figures 15 and 16 show the radial profiles of CH_4 and O_2 mass fractions, which represent the reactants of the system. The overall tendency of them is as expected, and the

Fig. 12 Mean and rms fluctuations of temperature for case A-r. \circ : experimental data; —: results on fine grid; - -: results on coarse grid; \bullet -: LES data extracted from Kuenne et al. [24]

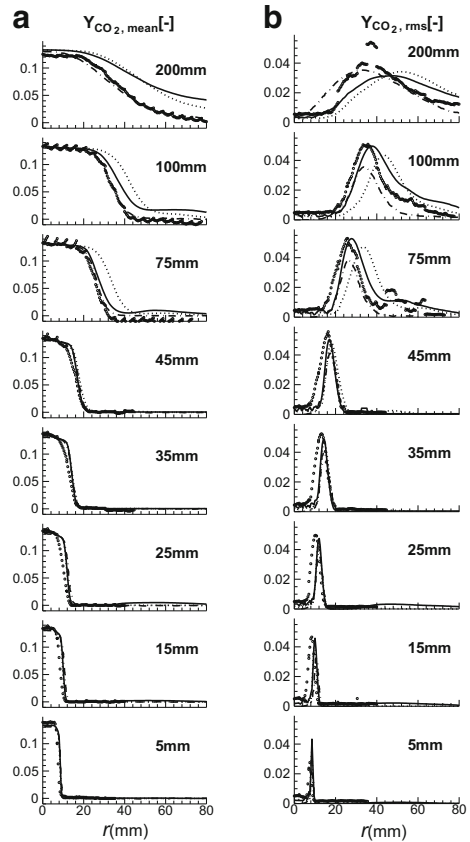


agreement between the LES results and experimental data is good. Stepwise variation of CH_4 is seen clearly at the lower axial locations by reason of the particularly arrangement of inflow reactant mixtures from the three pipes, as shown in Fig. 15a. Downstream of $x = 25$ mm, the steps become less obvious and the peak value starts to decrease. At further downstream $x = 200$ mm, it is found that there is still a small amount of methane remains in the exhaust gasses with a mean equivalence ratio approximately 0.3 and lower than the lean flammability limit.

The rms fluctuation profiles are shown in Figs. 12b–16b, unlike other quantities, with only one peak, the CH_4 profiles show a distinct triple-peak structure (Fig. 15b), which results from the above mentioned stepwise distribution of CH_4 . The inner peak with the highest peak value is corresponding to flame front position, whereas the two outer peaks are due to pure mixing of cold premixed reactants with different equivalence ratios. Since the outermost peak is corresponding to the mixing of gasses with $\varphi = 0.6$ and 0, while for the middle peak it is $\varphi = 0.9$ and 0.6, and it is expected that the outermost peak is higher than the middle one. The outer two peaks start to merge with the increase of distance from the pipe exit.

Similar to the temperature profiles, the LES results obtained with the fine grid show a better agreement with the experimental data for CO_2 , H_2O , CH_4 and O_2 , at the two axial locations, $x = 75$ mm and 100 mm (Figs. 13–16). It is also worth pointing out that this big discrepancy between the fine and coarse grid at these two axial locations is also presented

Fig. 13 Mean and rms fluctuations of CO₂ mass fraction for case A-r. “○”: experimental data; —: results on fine grid; - -: results on coarse grid; -•-: LES data extracted from Kuenne et al. [24]

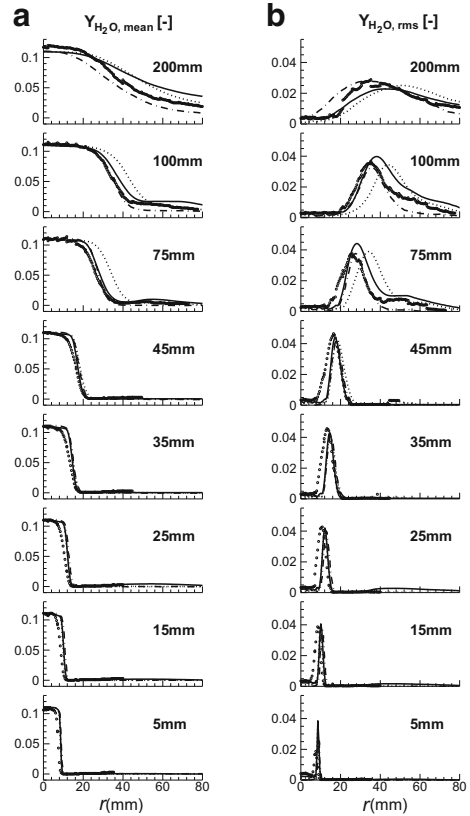


in [24]. Additionally, from the results displayed in Fig. A.18-A.25 of [11], it is clearly seen that the disagreement between the experimental data and the LES results obtained with 5 different SGS combustion models is also relatively larger at axial location $x = 75$ mm and 100 mm, compared with other locations. This phenomenon may suggest that the interaction between the stratified flame and turbulence in the range of $75 \text{ mm} < x < 100 \text{ mm}$ is more complex than in upstream and in downstream. In upstream, the reaction is very fast and flame front is thin, hence the cold mixture and hot pilot gas are separated fully; whereas in downstream, reaction is almost finished, and pure mixing is taking place. These two situations can be dealt with mature SGS combustion models, but for the situation in the range of $75 \text{ mm} < x < 100 \text{ mm}$, better performance model is needed.

5.3 Alignment of mixing layer and reaction layer

An important quantity in the turbulent stratified flames is the alignment of the mixing layer and the reaction layer, as illustrated in Fig. 1. In this work, this property is analyzed by calculating the probability distribution of the alignment angle, α , between the two gradient vectors of the resolved instantaneous temperature and equivalence ratio. It is worth pointing out that, in this alignment angle calculating procedure, only the resolved flow field information is accounted for. The unresolved fluctuation of equivalence ratio and flame wrinkling

Fig. 14 Mean and rms fluctuations of H_2O mass fraction for case A-r. ‘ \circ ’: experimental data; —: results on fine grid; - -: results on coarse grid; -·-: LES data extracted from Kuenne et al. [24]

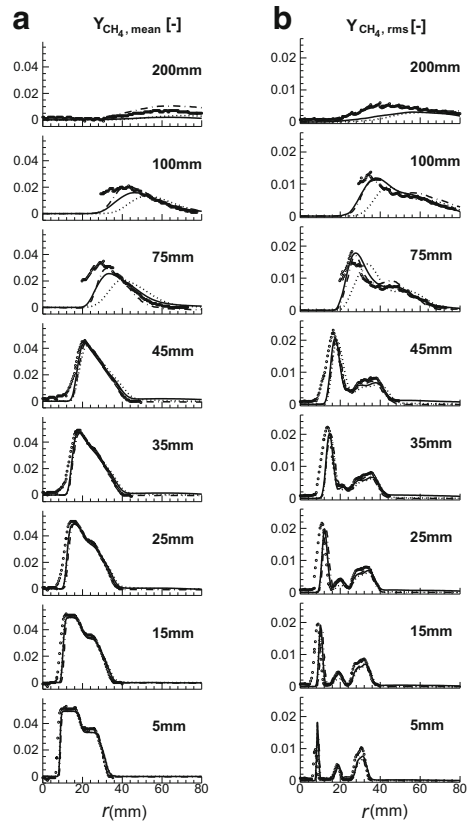


within the LES filtering volume is not taken into account. Recently, Wang et al. [61] investigated turbulent premixed swirling flames in a gas-turbine model combustor and found that the resolved flame surface area by LES is approximately 30%~40% of the real flame surface area. According to this conclusion, it is reasonable to assume that the unresolved flame wrinkling is also large for the flames considered in the present work. Therefore, the alignment angle, computed from the resolved instantaneous temperature and equivalence ratio, should be viewed as a volume averaged value for each LES filtering volume.

It is expected that the overall alignment angle should be approaching a small angle ($\alpha < \pi/2$) for the particular burner configuration, with hot exhaust gas from the pilot flame located in the center and cold coflow air surrounded the flame. In other words, the ‘back-supported’ combustion mode is expected to be dominant. Like the sampling method used in [24], only grid cells lying within the flame front are taken into account in the present work; therefore, a threshold of production rate of CO_2 above 100 s^{-1} is chosen. The perfectly premixed flame region is also excluded from sampling by using a condition that the equivalence ratio above 0.89, recalling that the highest value of equivalence ratio is 0.9 and located in the center pilot and slot 1. In addition, the sampling region is limited in $x > 40$ mm region.

Figure 17a shows a snapshot of the resolved instantaneous flame front ($T = 1500\text{K}$) in a cube region, colored by α . The center of the cube is located at $x = 87\text{mm}$, $r = 31\text{mm}$, and its size is 15 mm. It is seen that the flame front is highly wrinkled. The maximum

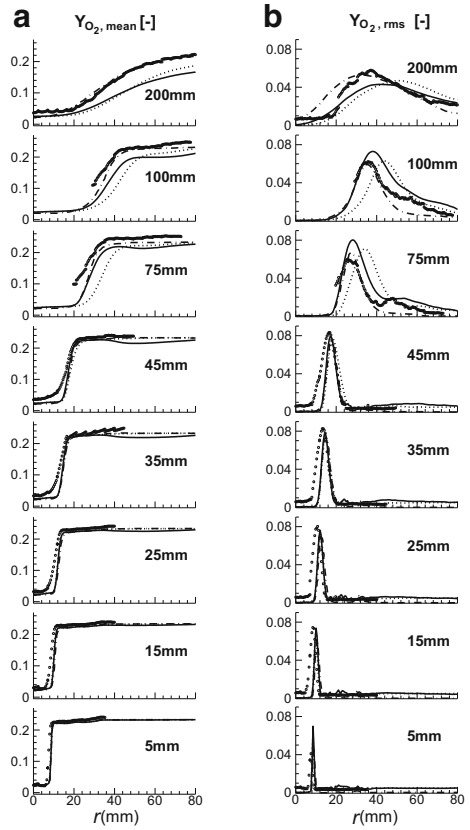
Fig. 15 Mean and rms fluctuations of CH₄ mass fraction for case A-r. ‘○’: experimental data; —: results on fine grid; - - results on coarse grid; -·- : LES data extracted from Kuenne et al. [24]



angle for this snapshot is as high as 2.4 rad, whereas the minimum angle is around 0.5 rad demonstrating both ‘front-supported’ ($\alpha > \pi/2$) and ‘back-supported’ ($\alpha < \pi/2$) flame situations are found for this snapshot. In order to analyze the delicate flow field around the point with maximum α , two slices of the same snapshot, showing color contours of temperature and equivalence ratio, respectively, are extracted from Fig. 17a and displayed in Fig. 17b. The isoline of $T = 1500\text{K}$ is used to represent the flame front. White arrows in Fig. 17b show the corresponding velocity direction on this slice. It is easy to find out that the alignment angle at intersection line of the two slices is larger than $\pi/2$, which is shown as a black point in Fig. 17b. This is caused by the strong wrinkling of flame front and the distorted mixing layer, which is a consequence of strong turbulence.

The time averaged probability distribution of α at different axial position intervals (e.g. $40\text{ mm} < x < 50\text{ mm}$) is analyzed carefully for all the reacting cases. The time averaging is performed by considering approximately 50 sample snapshots of the three-dimensional flame front (as shown in Fig. 9), with a time interval between two neighbor snapshots of about 0.7 milliseconds. In the considered Darmstadt TSF, the α varies from 0 to π , and all flame propagation modes of stratified flame, i.e., ‘back-supported’ ($\alpha < \pi/2$), normal ($\alpha = \pi/2$) and ‘front-supported’ ($\alpha > \pi/2$) can be found in the flow. Figure 18 shows sketches of these three modes. In the present work, the whole range of α is divided equally

Fig. 16 Mean and rms fluctuations of O₂ mass fraction for case A-r. $\circ\circ$: experimental data; —: results on fine grid; - - results on coarse grid; $\bullet\bullet$: LES data extracted from Kuenne et al. [24]



into 16 sections (e.g. $0 < \alpha < \pi/16$). The probability of the alignment angle is determined by accumulating the number of grid cells falling into each angle section within a certain axial position section, and then it is divided by the total number of grid cells.

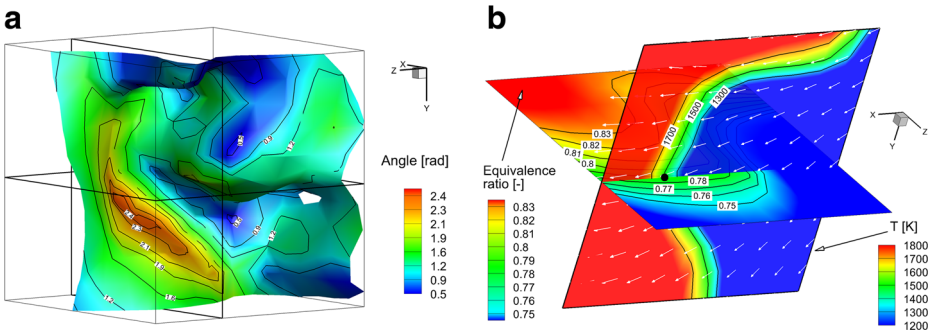


Fig. 17 Resolved instantaneous flame surface colored with alignment angle. **b** Two slices of the flow field of **(a)**, showing contours of temperature and equivalence ratio, respectively. White arrows are the velocity vector

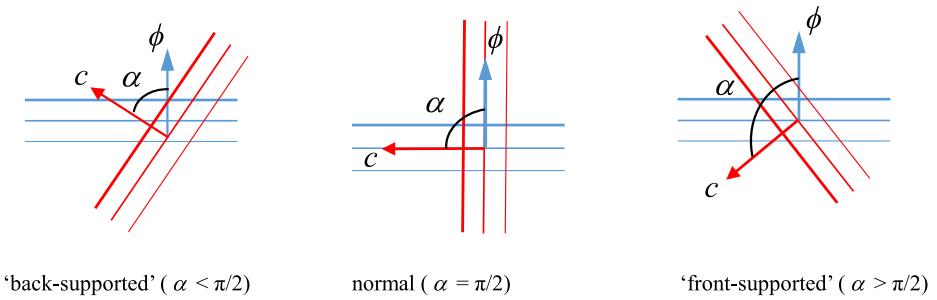


Fig. 18 Sketches of the three flame propagation modes of stratified flame. Arrows indicate the increase of the values according to the contour levels

It is shown in Fig. 19a that the probabilities of the alignment angle at different axial locations, for the case A-r (stratification but no shear), are completely different although all of them distribute widely and cover the whole range. A peak appears in the profile of position $x \in [40,50]$ mm, around $\alpha = 3.5\pi/16$. It is in this position, $x \in [40,50]$ mm, that

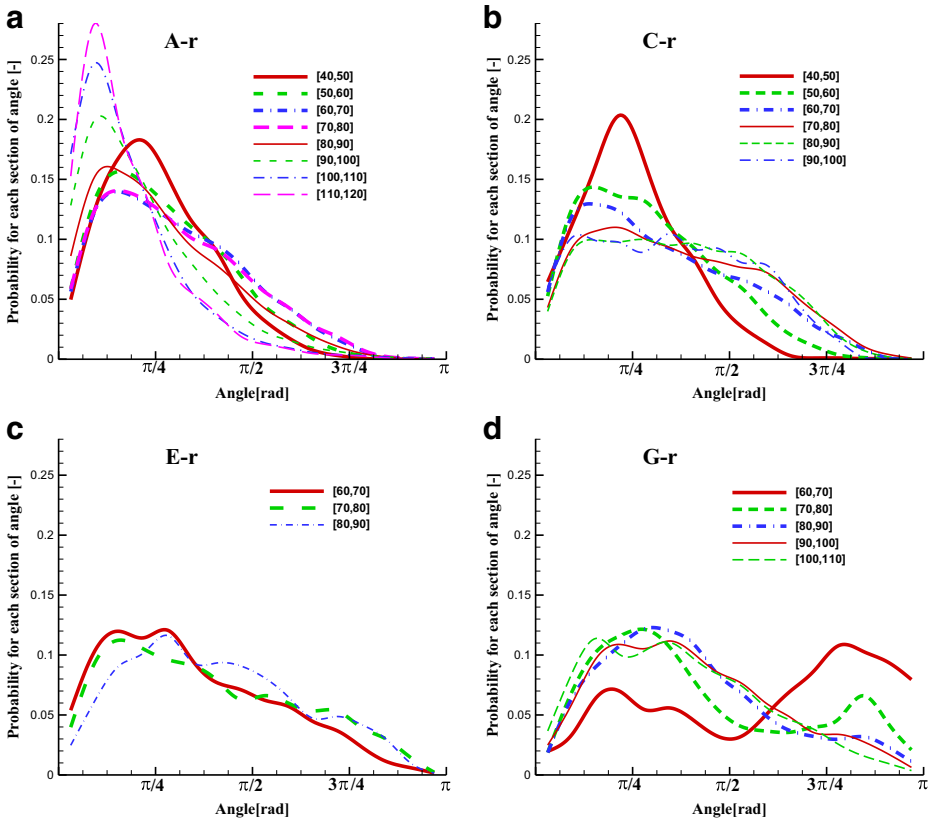


Fig. 19 Probability distributions of alignment angle at different axial position intervals, where numbers in the square brackets show the axial location range with a length unit mm

the flame front starts to cross the mixing layer (see Fig. 8a). The location of the peak is shifted toward $\alpha = 0$ side with the increase of axial distance from the nozzle. In other words, reaction layer and mixing layer become more and more parallel with axial distance from the nozzle increasing, which is similar to the finding of [24]. However, it is also interesting to note that in the axial range of $50 \text{ mm} < x < 90 \text{ mm}$, the probability for ‘front-supported’ flame propagating mode is increased slightly, compared with the profile for $x \in [40, 50]$ mm. This phenomenon is not reported in the LES of [24]. A reason might be that the flame wrinkling is increased in this region and, consequently, the α varies more in a small physical space.

Unlike the case A-r (stratification but no shear), a strong shear layer between the slot 1 and slot 2 (bulk velocity is 10 m/s and 5 m/s, respectively) is presented in the case C-r (stratification and shear). A faster mixing of the gasses from slot 1 and slot 2 can be obtained due to stronger turbulence induced by shear layer; therefore, the stratification effect is weaker in the case C-r. On the other hand, stronger turbulence can introduce more wrinkles on the flame front. It is seen in Fig. 19b that the probability for ‘back-supported’ flame propagating mode decreases continuously with the increase of axial distance from the nozzle, whereas the probability for ‘front-supported’ mode increases steadily, i.e., the distribution of probability in downstream tends to be flat. Based on the Fig. 19a and b, it is reasonable to conclude that the probability for finding ‘front-supported’ flame mode will be increased with a stronger turbulence, and the ‘back-supported’ and ‘front-supported’ flame modes are both important.

The arrangement of equivalence ratios in the case E-r (shear but no stratification) and G-r (neither shear nor stratification) is different from that of A-r and C-r, and stratification is only found between the coflow air and the slot 2 ($\varphi = 0.9$). Since the flames of E-r and G-r are propagating in the homogeneous reactant mixture with $\varphi = 0.9$ in upstream, there is no grid cell found with an effective alignment angle definition (gradient of φ is 0), so that the first probability distribution profile for E-r and G-r is only obtained in the region $x \in [60, 70]$ mm. The overall tendency of E-r (Fig. 19c) is similar to C-r (Fig. 19b), i.e., with the increase of axial distance from the nozzle, the probability for ‘back-supported’ flame mode decreases, whereas the probability for ‘front-supported’ mode increases.

It is shown in Fig. 19d that a peak of the probability profile for axial location in $x \in [60, 70]$ mm and $[70, 80]$ mm is found in the ‘front-supported’ side. This phenomenon can be explained by examining the corresponding flame movement of G-r (like the snapshot shown in Fig. 7d), in which the flame front is highly wrinkled and branches of the flame are even folded back. In region $60 \text{ mm} < x < 80 \text{ mm}$, the inner flame propagates in a perfect premixed mixture and only the outer flame transports in stratified mixture (propagating toward richer gas). It is natural to find a large number of grid cells with effective alignment angle larger than $\pi/2$, consequently, a big probability for ‘front-supported’ mode.

The time averaged probability distributions for the ‘whole’ region (its axial location range is shown in the square brackets) and for the four cases are displayed in Fig. 20. It is displayed that the major flame propagating mode for all the four cases is ‘back-supported’ flame. This is consistent with the particular flame configuration under consideration, in which the richer pilot flame ($\varphi = 0.9$) is located in the center, hence the flame front is propagating toward the outer leaner mixture ($\varphi = 0.6$) or the coflow air. Although all of the four profiles distribute widely and cover the whole range, their shapes are different. Based on the profiles shown in Fig. 20, the probability for ‘front-supported’ flame mode is 12%, 25%, 29% and 31% for the cases A-r, C-r, E-r and G-r, respectively. Especially for the case A-r (stratification but no shear), its probability distribution shows a much higher probability for ‘back-supported’ flame and the total probability for finding ‘front-supported’ flame

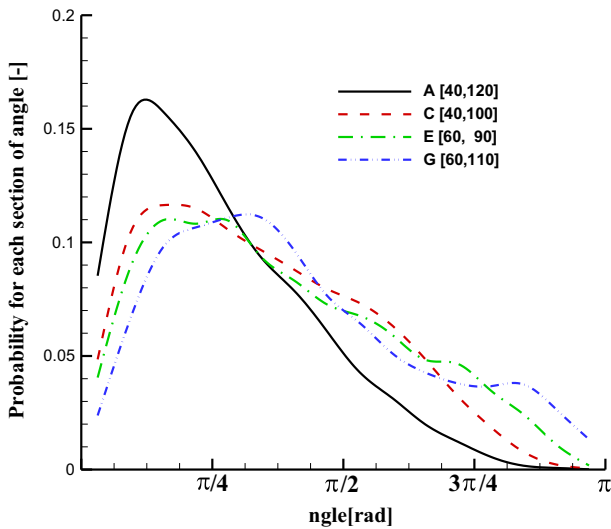


Fig. 20 Overall time averaged probability distributions of alignment angle for the four reacting cases, where numbers in the square brackets show the axial location range with a length unit mm

mode is only 12%. For the other three cases, the probability for the ‘back-supported’ flame transporting mode decreases a lot, and the ‘front-supported’ flame mode consists a more important contribution to the whole flame propagating manner.

6 Concluding Remarks

The REDIM-PFDF SGS combustion model is used to simulate the TU-Darmstadt turbulent stratified flames: A-r, C-r, E-r, G-r. In the model, the chemistry is accounted for by a two-dimensional chemistry look-up table, generated by the novel REDIM technology for reducing chemical kinetics, while the fluctuation of scalars within the LES filter volume is modeled by the presumed FDF approach. For the identification of the look-up table, a detailed mechanism for methane combustion was used and equal diffusivities of the species and unity Lewis number were assumed, which is an acceptable simplification for methane combustion. The used two-dimensional look-up table in the present work is coordinated with the mass fractions of N_2 and CO_2 . The assumption of statistical independence of N_2 and CO_2 is employed in this work, which leads to the joint FDF being equal to the product of the two marginal FDFs. Unlike in [35] β -FDF was used for both the SGS distributions of mixture fraction and the progress variable, in the present work the SGS distributions of N_2 and CO_2 are both presumed to be of Clipped Gaussian shape.

Statistic results are obtained for the isothermal case A-i2 and reacting case A-r (with strong stratified effect and weak shear layer), and they are compared to the experimental data. The overall good agreement of the statistics of velocity, temperature and species with the experimental data demonstrates the capability of the REDIM-PFDF model to cope with turbulent stratified flame. At the two axial stations $x = 75$ mm and 100 mm, the fine grid predicted a better agreement with the experimental data than the coarse grid, which reveals the preference of finer grid in predicting the strong interaction between reaction and strong stratification.

In the present work, the used two-dimensional chemistry look-up table did not account for heat loss effects so that the temperature was predicted to be higher than the measured temperature, i.e., close to the exit of pilot pipe. For the set-up under consideration, the heat-loss only occupies a small percentage of the whole heat-release. The neglected heat-loss effect cannot change the overall flame behavior substantially. The conclusions of the present paper are still correct. It is possible to account for heat losses (including radiative heat loss) within the REDIM reduced chemistry table as well. This has been shown for applications of the method [62, 63]. However, for the stratified combustion considered here, this would require a further dimension of the manifold, and it was omitted at this stage for the sake of simplicity.

The stratification effect is analyzed by checking the alignment angle between the resolved instantaneous mixing layer and reaction layer. The probability distribution of alignment angle is calculated for different axial locations. It is found that the probability distributions of the alignment angle vary with the axial distance from the jet nozzle. In case A-r, the location of the peak of distribution profile is shifted toward $\alpha = 0$ side with the increase of axial distance from the nozzle, i.e., ‘back-supported’ flame mode becomes more dominant. This tendency is changed if a stronger shear layer introduced in the flow field, e.g., in the case C-r. With a stronger turbulence induced by the shear layer, the mixing of gasses with different equivalence ratio is faster, and hence the stratification effect is weaker. At the same time, stronger turbulence can introduce more wrinkles on the flame front and, consequently, alignment angle varies greatly in a small physical domain. This finally tends to improve the probability for ‘front-supported’ flame mode, and hence the difference between the probabilities for ‘back-supported’ and ‘front-supported’ decreases.

Acknowledgments The support of Natural Science Foundation of China through project 51576092 and 91741117, the support of Natural Science Foundation of Jiangsu Province through project BK20151344, and the support of PAPD project funded by Jiangsu Higher Education Institution are gratefully acknowledged. Furthermore, funding by the DFG in the frame of the SFB/TR150 is acknowledged. The authors also thank Prof. A. Dreizler and his team (Technical University of Darmstadt, Germany) for providing the experimental results in electronic form.

Funding Information This study was funded by Natural Science Foundation of China (51576092, 91741117), Natural Science Foundation of Jiangsu Province (BK20151344), PAPD project of Jiangsu Higher Education Institution, as well as the DFG (SFB/TR150).

Compliance with Ethical Standards

Conflict of interests The authors declare that they have no conflict of interest.

Publisher’s Note Springer Nature remains neutral with regard to jurisdictional claims in published maps and institutional affiliations.

References

1. Lieuwen, T., Zinn, B.T.: The role of equivalence ratio oscillations in driving combustion instabilities in low NO_x gas turbines. *Proc. Combust. Inst.* **27**(2), 1809–1816 (1998)
2. Masri, A.R.: Partial premixing and stratification in turbulent flames. *Proc Combust. Inst.* **35**(2), 1115–1136 (2015)
3. Gong, C., Jangi, M., Bai, X.S.: Large eddy simulation of n-Dodecane spray combustion in a high pressure combustion vessel. *Appl. Energy* **136**, 373–381 (2014)

4. Gövert, S., Mira, D., Kok, J.B., Vázquez, M., Houzeaux, G.: Turbulent combustion modelling of a confined premixed jet flame including heat loss effects using tabulated chemistry. *Appl. Energy* **156**, 804–815 (2015)
5. Nambully, S., Domingo, P., Moureau, V., Vervisch, L.: A filtered-laminar-flame PDF sub-grid-scale closure for LES of premixed turbulent flames: II. Application to a stratified bluff-body burner. *Combust. Flame* **161**(7), 1775–1791 (2014)
6. Ghania, A., Poinso, T., Gicquel, L., Staffelbach, G.: LES of longitudinal and transverse self-excited combustion stabilities in a bluff-body stabilized turbulent premixed flame. *Combust. Flame* **162**(11), 40754083 (2015)
7. Yang, Y., Wang, H., Pope, S.B., Chen, J.H.: Large-eddy simulation/probability density function modeling of a non-premixed CO/H₂ temporally evolving jet flame. *Proc. Combust. Inst.* **34**(1), 241–249 (2013)
8. Volpiani, P.S., Schmitt, T., Veynante, D.: Large eddy simulation of a turbulent swirling premixed flame coupling the TFLES model with a dynamic wrinkling formulation. *Combust. Flame* **180**, 124–135 (2017)
9. Bulat, G., Jones, W.P., Marquis, A.J.: NO and CO formation in an industrial gas-turbine combustion chamber using LES with the Eulerian sub-grid PDF method. *Combust. Flame* **161**, 1804–1825 (2014)
10. Goryntsev, D., Sadiki, A., Janicka, J.: Analysis of misfire processes in realistic Direct Injection Spark Ignition engine using multi-cycle Large Eddy Simulation. *Proc. Combust. Inst.* **34**(2), 2969–2976 (2013)
11. Fiorina, B., Mercier, R., Kuenne, G., Ketelheun, A., Avdić, A., Janicka, J., Geyer, D., Dreizler, A., Alenius, E., Duwig, C., Trisjono, P., Kleinheinz, K., Kang, S., Pitsch, H., Proch, F., Kempf, A., Marincola, C.: Challenging modeling strategies for LES of non-adiabatic turbulent stratified combustion. *Combust. Flame* **162**(11), 4264–428 (2015)
12. Sun, W., Ju, Y.: A multi-timescale and correlated dynamic adaptive chemistry and transport (CO-DACT) method for computationally efficient modeling of jet fuel combustion with detailed chemistry and transport. *Combust. Flame* **184**(10), 297311 (2017)
13. Bravo, L., Wijeyakulasuriya, S., Pomraning, E., Senecal, P.K., Kweon, C.: Large eddy simulation of high Reynolds number nonreacting and reacting JP-8 sprays in a constant pressure flow vessel with a detailed chemistry approach. *J. Energy Resour. Technol.* **138**(5), 032207 (2016)
14. Filosa, A., Noll, B.E., Domenico, M.D., Aigner, M.: Numerical investigations of a low emission gas turbine combustor using detailed chemistry. *Propulsion and Energy Forum*, Cleveland (2014). 50th AIAA/ASME/SAE/ASEE Joint Propulsion Conference
15. Lu, T.F., Law, C.K.: Toward accommodating realistic fuel chemistry in large-scale computations. *Prog. Energy Combust. Sci.* **35**(2), 192–215 (2009)
16. Goussis, D.: Turbulent Combustion Modeling. In: Maas, U., Echehki, T., Mastorakos, E. (eds.) *Fluid Mechanics and its Applications*, pp. 193–220 (2011)
17. Tomlin, A.S., Turányi, T., Pilling, M.J.: Chapter 4 Mathematical tools for the construction, investigation and reduction of combustion mechanisms. *Cheminform* **29**, 293–437 (1998)
18. Bykov, V., Maas, U.: Problem adapted reduced models based on Reaction–Diffusion Manifolds (REDIMs). *Proc. Combust. Inst.* **32**(1), 561–568 (2009)
19. Steinhilber, G., Maas, U.: Reaction-diffusion manifolds for unconfined, lean premixed, piloted, turbulent methane/air systems. *Proc. Combust. Inst.* **34**(1), 217–224 (2013)
20. Maas, U., Pope, S.B.: Simplifying chemical kinetics: intrinsic low-dimensional manifolds in composition space. *Combust. Flame* **88**(3), 239–264 (1992)
21. Gicquel, O., Darabiha, N., Thévenin, D.: Laminar premixed hydrogen/air counterflow flame simulations using flame prolongation of ILDM with differential diffusion. *Proc. Combust. Inst.* **28**(2), 1901–1908 (2000)
22. Van Oijen, J., Lammers, F., De Goey, L.P.H.: Modeling of complex premixed burner systems by using flamelet-generated manifolds. *Combust. Flame* **127**(3), 2124–2134 (2001)
23. Nguyen, P., Vervisch, L., Subramanian, V., Domingo, P.: Multidimensional flamelet-generated manifolds for partially premixed combustion. *Combust. Flame* **157**(1), 43–61 (2010)
24. Kuenne, G., Seffrin, F., Fuest, F., Stahler, T., Ketelheun, A., Geyer, D., Janicka, J., Dreizler, A.: Experimental and numerical analysis of a lean premixed stratified burner using 1D Raman/Rayleigh scattering and large eddy simulation. *Combust. Flame* **159**(8), 2669–2689 (2012)
25. Cruz, A.P., Dean, A., Grenda, J.M.: A numerical study of the laminar flame speed of stratified methane/air flames. *Proc. Combust. Inst.* **28**(2), 1925–1932 (2000)
26. Jiménez, C., Cuenot, B., Poinso, T., Haworth, D.: Numerical simulation and modeling for lean stratified propane-air flames. *Combust. Flame* **128**(1), 1–21 (2002)
27. Bonaldo, A., Kelman, J.B.: Experimental annular stratified flames characterisation stabilised by weak swirl. *Combust. Flame* **156**(4), 750–762 (2009)
28. Sweeney, M., Hochgreb, S., Dunn, M., Barlow, R.S.: The structure of turbulent stratified and premixed methane/air flames I: Non-swirling flows. *Combust. Flame* **159**(9), 2896–2911 (2012)

29. Barlow, R., S Meares, G., Magnotti, H., Cutcher, A.R.: Masri, Local extinction and near-field structure in piloted turbulent CH₄/air jet flames with inhomogeneous inlets. *Combust. Flame* **162**(10), 3516–3540 (2015)
30. Seffrin, F., Fuest, F., Geyer, D., Dreizler, A.: Flow field studies of a new series of turbulent premixed stratified flames. *Combust. Flame* **157**(2), 384–396 (2010)
31. Böhm, B., Frank, J., Dreizler, A.: Temperature and mixing field measurements in stratified lean premixed turbulent flames. *Proc Combust. Inst.* **33**(1), 1583–1590 (2011)
32. Roux, A., Pitsch, H.: Large-eddy simulation of stratified combustion. Center for Turbulence Research Annual Research Briefs, pp 275–288 (2010)
33. Avdić, A., Kuenne, G., Ketelheun, A., Sadiki, A., Jakirlić, S., Janicka, J.: High performance computing of the Darmstadt stratified burner by means of large eddy simulation and a joint ATF-FGM approach. *Comput. Vis. Sci.* **16**(2), 77–88 (2013)
34. Marincola, F.C., Ma, T., Kempf, A.M.: Large eddy simulations of the Darmstadt turbulent stratified flame series. *Proc. Combust. Inst.* **34**(1), 1307–1315 (2013)
35. Trisjono, P., Kleinheinz, K., Pitsch, H., Kang, S.: Large eddy simulation of stratified and sheared flames of a premixed turbulent stratified flame burner using a flamelet model with heat loss. *Flow Turbul. Combust.* **92**(1-2), 201–235 (2014)
36. Mercier, R., Auzillon, P., Moureau, V., Darabiha, N., Gicquel, O., Veynante, D., Fiorina, B.: LES modeling of the impact of heat losses and differential diffusion on turbulent stratified flame propagation: application to the TU Darmstadt stratified flame. *Flow Turbul. Combust.* **93**(2), 349–381 (2014)
37. Wang, P., Platova, N., Fröhlich, J., Maas, U.: Large Eddy Simulation of the PRECCINSTA burner. *Int. J. Heat. Mass. Transf.* **70**, 486–495 (2014)
38. Wang, P., Zieker, F., Schießl, R., Platova, N., Fröhlich, J., Maas, U.: Large Eddy Simulations and experimental studies of turbulent premixed combustion near extinction. *Proc. Combust. Inst.* **34**(1), 1269–1280 (2013)
39. Warnatz, J., Maas, U., Dibble, R.W., Warnatz, J. *Combustion*, 4th edn. Springer-Verlag, Berlin (2001)
40. Donini, A., Bastiaans, R.J.M., Oijen, J.A.V., De Goey, L.P.H.: Differential diffusion effects inclusion with flamelet generated manifold for the modeling of stratified premixed cooled flames. *Proc. Comb. Inst.* **35**(1), 831–837 (2015)
41. Maas, U., Bykov, V.: The extension of the reaction/diffusion manifold concept to systems with detailed transport models. *Proc. Comb. Inst.* **33**(1), 1253–1259 (2011)
42. Knudsen, E., Pitsch, H.: Large-eddy simulation for combustion systems: modeling approaches for partially premixed flows. In: *Proceedings of the Australian Combustion Symposium, 2009*. The University of Queensland, Australia (2009)
43. Knudsen, E., Pitsch, H.: Capabilities and limitations of multi-regime flamelet combustion models. *Combust. Flame* **159**(1), 242–264 (2012)
44. Ukai, S., Kronenburg, A., Stein, O.T.: Large eddy simulation of dilute acetone spray flames using CMC coupled with tabulated chemistry. *Proc. Combust. Inst.* **35**(2), 1667–1674 (2015)
45. Sundaram, B., Klimenko, A.Y.: A PDF approach to thin premixed flamelets using multiple mapping conditioning. *Proc. Combust. Inst.* **36**, 1937–1945 (2017)
46. Lipp, S., Magagnato, F., Maas, U.: A hybrid transported PDF/CFD model for turbulent flames using REDIM. In: *Proceedings of the 4th European Combustion Meeting*, pp. 810103 (2009)
47. Merci, B., Naud, B., Roekaerts, D., Maas, U.: Joint scalar versus joint velocity-scalar PDF simulations of bluff-body stabilized flames with REDIM. *Flow Turbul. Combust.* **82**(2), 185–209 (2009)
48. Floyd, J., Kempf, A.M., Kronenburg, A., Ram, R.H.: A simple model for the filtered density function for passive scalar combustion LES. *Combust. Theor. Model.* **13**(4), 559–588 (2009)
49. Kempf, A., Kronenburg, A.: LES of a non-premixed flame with an assumed tophat PDF, *Adv. Turbul. XII*, pp. 763–766. Springer, Berlin (2009)
50. Bondi, S., Jones, W.: A combustion model for premixed flames with varying stoichiometry. *Proc. Combust. Inst.* **29**(2), 2123–2129 (2002)
51. Kuehne, J., Ketelheun, A., Janicka, J.: Analysis of sub-grid PDF of a progress variable approach using a hybrid LES/TPDF method. *Proc. Combust. Inst.* **33**(1), 1411–1418 (2011)
52. Galpin, J., Naudin, A., Vervisch, L., Angelberger, C., Colin, O., Domingo, P.: Large-eddy simulation of a fuel-lean premixed turbulent swirl-burner. *Combust. Flame.* **155**(1), 247–266 (2008)
53. Meier, W., Weigand, P., Duan, X., Giezendanner, T.R.: Detailed characterization of the dynamics of thermoacoustic pulsations in a lean premixed swirl flame. *Combust. Flame.* **150**(1), 2–26 (2007)
54. Jiménez, J., Liñán, A., Rogers, F.J.: Higuera A priori testing of subgrid models for chemically reacting non-premixed turbulent shear flows. *J. Fluid. Mech.* **349**, 149–171 (1997)
55. Mare, F., Jones, W., Menzies, K.R.: Large eddy simulation of a model gas turbine combustor. *Combust. Flame.* **137**(3), 278–294 (2004)

56. Landenfeld, T., Sadiki, A., Janicka, J.: A turbulence-chemistry interaction model based on a multivariate presumed beta-pdf method for turbulent flames. *Flow Turbulence. Combust.* **68**(2), 111–135 (2002)
57. Wang, P., Fröhlich, J., Michelassi, V., Rodi, W.: Large-eddy simulation of variable-density turbulent axisymmetric jets. *Int. J. Heat. Fluid. Flow.* **29**(3), 654–664 (2008)
58. Zhu, J.: A low-diffusive and oscillation-free convection scheme. *Int. J. Numer. Methods Biomed. Eng.* **7**(3), 225–232 (1991)
59. Werner, H., Wengle, H.: Large-eddy simulation of turbulent flow over and around a cube in a plate channel. *Turbulent Shear Flows* 8, pp. 155–168. Springer, Berlin (1993)
60. Wang, P., Bai, X.S.: Large eddy simulation of turbulent premixed flames using level-set G-equation. *Proc. Comb. Inst.* **30**(1), 583–591 (2005)
61. Wang, P., Fröhlich, J., Maas, U., He, Z.X., Wang, C.J.: A detailed comparison of two sub-grid scale combustion models via large eddy simulation of the PRECCINSTA gas turbine model combustor. *Combust. Flame* **164**(2), 329–345 (2016)
62. Ghorbani, A., Steinhilber, G., Markus, D., Maas, U.: Numerical investigation of ignition in a transient turbulent jet by means of a PDF method. *Combust. Sci. Tech.* **186**(10-11), 1582–1596 (2014)
63. Steinhilber, G., Bykov, V., Maas, U.: REDIM reduced modeling of flame-wall-interactions: Quenching of a premixed methane/air flame at a cold inert wall. *Proc. Combust. Inst.* **36**(1), 655 (2017)